Research Article Vol. 31, No. 1 / 2 Jan 2023 / Optics Express 459
Optics EXPRESS

Underwater polarization imaging for visibility enhancement of moving targets in turbid environments

TAO YU,[1] XIAOLEI WANG,[2,5] SIXING XI,[3,6] QUANQUAN MU,[4] AND ZHUQING ZHU[1,4,*]

[1]School of Physical Science and Technology, School of Computer and Electronic Information, Nanjing Normal University, Nanjing 210023, China
[2]Institute of Modern Optics, Tianjin Key Laboratory of Micro-scale Optical Information Science and Technology, Nankai University, Tianjin 300350, China
[3]School of Mathematics and Physics Science and Engineering, Hebei University of Engineering, Handan, Hebei 056038, China
[4]State Key Laboratory of Applied Optics, Changchun Institute of Optics, Fine Mechanics and Physics, Chinese Academy of Sciences, Changchun 130033, China
[5]wangxiaolei@nankai.edu.cn
[6]xisixing@126.com
[*]zhuqingzhu@njnu.edu.cn

Abstract: Polarization imaging techniques have more prominent advantages for imaging in strongly scattered media. Previous de-scattering methods of polarization imaging usually require the priori information of the background region, and rarely consider the effect of non-uniformity of the optical field on image recovery, which not only reduces the processing speed of imaging but also introduces errors in image recovery, especially for moving targets in complex scattering environments. In this paper, we propose a turbid underwater moving image recovery method based on the global estimation of the intensity and the degree of polarization (DOP) of the backscattered light, combined with polarization-relation histogram processing techniques. The full spatial distribution of the intensity and the DOP of the backscattered light are obtained by using frequency domain analysis and filtering. Besides, a threshold factor is set in the frequency domain low-pass filter, which is used to adjust the execution region of the filter, which effectively reduces the error in image recovery caused by estimating the DOP of the backscattered light as a constant in traditional methods with non-uniform illumination. Meanwhile, our method requires no human-computer interaction, which effectively solves the drawbacks that the moving target is difficult to be recovered by traditional methods. Experimental studies were conducted on static and moving targets under turbid water, and satisfactory image recovery quality is achieved.

1. Introduction

Underwater optical imaging techniques has the great applications in marine resource exploration [1], seafloor topography exploration [2] and underwater ecological environment monitoring [3]. However, the severe effects resulting from the absorption and scattering of suspending particles in water always causes a dramatic degradation of the imaging quality [4]. Therefore, it is an urgent problem for underwater imaging to further suppress the interference of scattered light in turbid water environment and extract more effective target information.

Based on the uniqueness and difference of the polarization state of light between targets and water, polarization imaging has emerged as an effective method of suppressing backscattered light to obtain clear underwater images [5–9]. Schechner [10,11] proposed an underwater passive polarization imaging method utilizing the atmospheric scattering model to recover clear underwater images, which treated the target light as non-polarized. Huang [12] then considered

#477243 https://doi.org/10.1364/OE.477243
Journal © 2023 Received 6 Oct 2022; revised 2 Dec 2022; accepted 5 Dec 2022; published 21 Dec 2022

Optics EXPRESS

the degree of polarization (DOP) of the target light and obtained better recovery results by accurately deriving the scene transmittance. To further improve the quality of underwater imaging, Treibitz and Schechner [13] introduced active illumination to establish the active underwater polarization imaging model, which realized the effective separation of background and target information with active illumination. Zhao [14] utilized genetic algorithm to search the DOP of the target light and the backscattered light simultaneously and acquired good de-scattering effect without priori information. However, this method considers the DOP of the backscattered light to be uniform, while in practice the intensity and DOP of the backscattered light are not uniformly distributed, which lead to poor image recovery. Hu [15] skillfully employed the extrapolation method and least squares method to estimate the spatial distribution of the DOP and intensity of the backscattered light, and considerably improved the quality of underwater image. But time-consuming manual selection for the background region is required, which will hinder real-time detection and processing in underwater polarization imaging.

In this paper, we propose an underwater polarization imaging method for visibility enhancement of moving targets in turbid environments based on the Schechner's active polarization imaging model [13]. The full spatial distribution of the backscattered light's intensity and DOP are firstly estimated by frequency-domain low-pass filtering with optimal threshold factor meanwhile the target light's DOP is calculated by using the image evaluation index. At the same time, histogram stretching preprocessing technique of polarization relation [16] is used to obtain the polarized images with a larger gray scale. Finally, the DOP of the backscattered light and the target light are substituted into the model to obtain the recovery images. The experimental results show that the restored static targets are clearly distinguishable and the corresponding image evaluation indexes are greatly improved. Especially, moving targets under non-uniform illumination environment are also clearly recovered.

2. Theory

Generally, the underwater images received by the detector can be considered as an incoherent superposition of the target light and the backscattered light. The target light is the clear target image we eventually want to get, which mainly contains the diffuse reflected light. The backscattered light comes from the scattering effect of surrounding environment, which is mainly caused by the particles in the water. Based on traditional underwater active polarization imaging models [13], a clear underwater image can be modeled by

$$S = \frac{1}{P_{sca} - P_{obj}}[I_{\perp}(1 + P_{sca}) - I_{\parallel}(1 - P_{sca})], \tag{1}$$

where S represents the target light, $I_{\parallel}$ and $I_{\perp}$ are the intensity of a pair of orthogonal polarized images, P_{sca} and P_{obj} are the DOP of the backscattered light and the target light respectively. Based on the assumption that DOP of backscattered light as a constant, the DOP of the backscattered light is often obtained by manually selected a target-free background region [10], which can be expressed as

$$\widehat{P}_{sca} = \sum \frac{I_{\parallel}(\Omega) - I_{\perp}(\Omega)}{I_{\parallel}(\Omega) + I_{\perp}(\Omega)} / N(\Omega), \tag{2}$$

where $\widehat{P}_{sca}$ the average of the DOP in selected background region indicates, Ω is the selecting background region, $N(\Omega)$ is the total pixel number in the background region.

But, the intensity and DOP distribution of backscattered light are non-uniform in realistic turbid environments for the varying attenuation of the active illumination source caused by random scattering, which will get worse with the increase of transmission distance. Therefore

Optics EXPRESS

Eq. (2) should be modified as [17]

$$P_{sca} = \frac{(I_{\parallel} - I_{\perp}) - P_{obj}[(I_{\parallel} + I_{\perp}) - \hat{B}]}{\hat{B}}, \tag{3}$$

where $\hat{B}$ denotes the whole intensity of the backscattered light.

Considering the low frequency characteristic of the backscattered light [18], we perform frequency-domain low-pass filtering [19] on the entire image to accurately estimate the whole intensity $\hat{B}$ instead of selecting a target-free background region for calculation. The process is that the intensity image is first transformed to the frequency domain by the Fourier function and then multiplied with the filter's transfer function, the result of the multiplication is then returned to the spatial domain image by the inverse Fourier transform.

$$\hat{B} = \mathcal{F}^{-1}\{\mathcal{F}\{I_{\parallel} + I_{\perp}\} \times H(\mathrm{u,v})\}, \tag{4}$$

where $\mathcal{F}$ and $\mathcal{F}^{-1}$ denote the Fourier transform and the Fourier inverse transform. The transfer function of the frequency filter is given by

$$H(u, v) = \frac{1}{1 + (D(u, v)/D_0)^{2\lambda}}, \tag{5}$$

where $D(u, v)$ is the distance from the data point to the center in the frequency domain, D_0 is the cut-off frequency and λ is the order of the filter. In this paper, we set the cut-off frequency as $D_0 = 50Hz$ and the order of the filter as $\lambda = 2$.

However, this method has some effect on the low contrast region of the target, that is, the backscattered light intensity obtained by the low-pass filtering on these low contrast regions will have some errors. To further improve the contrast of image areas with detailed information, we introduce a threshold to improve the accuracy of the estimated filter. The difference between the whole intensity of the backscattered light and the original image intensity is defined as

$$\begin{aligned} DIFF &= |\hat{B} - (I_{\parallel} + I_{\perp})| \\ &= |\hat{B} - I|, \end{aligned} \tag{6}$$

where I indicates the intensity of the initial image.

We set a threshold factor σ to improve the accuracy of the frequency domain low-pass filter. When the $DIFF{>}\sigma$, the low-pass filtered result is kept as the intensity of the backscattered light. In contrast, the intensity of original image remains unchanged when $DIFF \leq \sigma$. The implement process is described as:

$$\begin{cases} \hat{B}^{opt}(x, y) = \hat{B}(x, y), \ DIFF{>}\sigma \\ \hat{B}^{opt}(x, y) = I(x, y), \ DIFF \leq \sigma \end{cases}, \tag{7}$$

where (x, y) represents the pixel position, $\hat{B}^{opt}$ is the optimized backscattered light intensity.

For the optimized estimation of P_{obj}, we use the measure of enhancement (EME [20]) to evaluate the effect for de-scattering. A high EME value indicates high image quality. As a non-reference evaluation metric, EME can accurately evaluate image quality quantitatively in most cases. Therefore, we search for the optimal value of the P_{obj} in steps of 0.01 within [0, 1] and the value of σ in steps of 0.01 within [0, 0.3] at the same time:

$$\begin{aligned} (\sigma, P_{obj})^{optimal} &= \arg\max\{EME(S)\} \\ &= \arg\max \frac{1}{mn} \sum_{k_2=1}^{m} \sum_{k_1=1}^{n} 20 \log \frac{S_{\max;k_1,k_2}}{S_{\min;k_1,k_2}}, \end{aligned} \tag{8}$$

where the image is divided into $m \times n$ areas with the ordinal number (k_1, k_2), $S_{\max;k_1,k_2}$ and $S_{\min;k_1,k_2}$ are the maximum and minimum values of image grayscale for each area respectively.

Optics EXPRESS

Here we divided the image into 300×300 areas to calculate the EME values, so the values of k_1 and k_2 are from 1 to 300.

With the increase of the scattering environment turbidity, the interference of the backscattered light will result in the imaging grayscale range sharply compressed, which make the desired recovery worse. Therefore, we introduce the method of stretching histogram with polarization relation proposed by Li [16] to preprocess two orthogonal polarization images, the intensity histograms of a polarized image are firstly stretched, and then another polarized image is calculated by polarization correlation of the whole scene. This method stretches the histograms of the two orthogonal polarized images while maintaining the degree of polarization of the scene unchanged. Instead of the original images, the two processed orthogonal images are applied to obtain final reconstruction results.

The whole image processing is illustrated as Fig. 1. Firstly, the two experimental acquired orthogonal polarized images are superimposed to get the intensity of scene image, and the frequency-domain low-pass filtering is performed on the intensity image to estimate the intensity of backscattered light. Then the estimation of the backscattered light's DOP can be obtained by Eq. (3) meanwhile the optimal value of the threshold factor and the target light's DOP are iteratively computed by Eq. (8). Finally, the clear recovery result can be obtained by substituting the estimated parameters and the original polarized images after stretching histogram with polarization relation into Eq. (1).

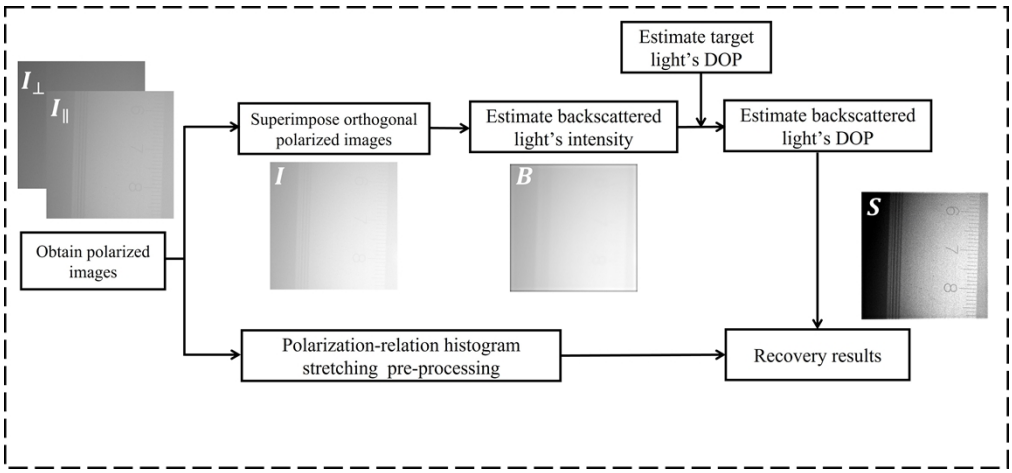

Fig. 1. Principal flow diagram of the polarization de-scattering algorithm.

3. Experiments and results

The experimental setup for underwater polarization imaging is shown in Fig. 2. The light emitted from the white LED source passing through the diaphragm and the polarizer hits the target under turbid water with horizontal polarization state. The angle between the source LED and PPC is set around 30°, this angle has been as far as possible to avoid the direct reflection of light. Two underwater target images with orthogonal polarization states are recorded by a pixelated polarization camera (BFS-U3-51S5P-C, 2448*2048) at the same time. The lens focal length of camera is 12 mm and the turbid images in this paper were acquired under the conditions of exposure time of 80-100 ms. In this paper, we do not consider the effect of the glass boundary on polarization because we focus on the image recovery method under different turbidity degrees, in which the conditions of the container are unchanged with the varying turbidity of the environment.

Optics EXPRESS

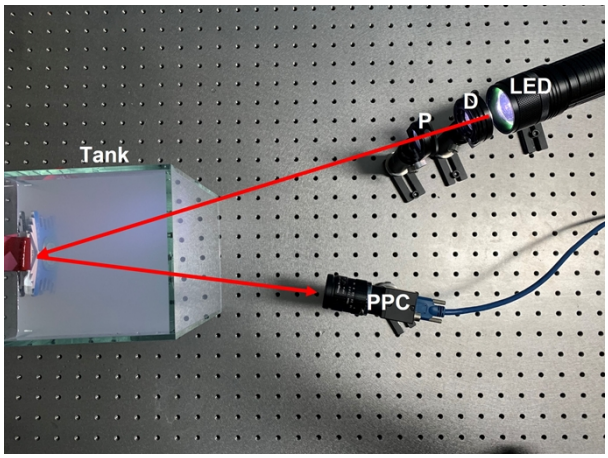

Fig. 2. Polarization imaging experimental setup. D: diaphragm, P: polarizer, Tank: thin glass material, PPC: pixelated polarization camera.

To simulate the underwater environment with different scattering levels, different amounts of whole milk with protein content of 2.9 g/100 mL and fat content of 3.1 g/100 mL are injected into the water. We mixed milk in a tank with 4 L water to simulate three different levels of turbidity (milk concentration relative to water at 1 g/L, 1.5 g/L, 2 g/L), and an iron medallion is first selected to evaluate the scattering suppression of the same target in different turbid environments with our proposed method. For comparison, CLAHE [21] and Schechner's active polarization imaging technique are also chosen. CLAHE is a variant of adaptive histogram equalization in which the contrast amplification is limited, thereby resulting in reduction of noise amplification and it is a simple digital image processing method to enhance the contrast of images which have a good effect on image enhancement. The corresponding recovery results are shown in Fig. 3 respectively.

It can be seen from Figs. 3(a) and (b) that the clarity and contrast of the original image has been greatly improved, in which the medal details, such as the words of 'NNU' and patterns, are clearly distinguishable. Although the contrast of CLAHE's recovery images is somewhat enhanced as shown in Fig. 3(c), the curtain effect caused by scattered particles has not been well resolved. For the results of Schechner's method shown in Fig. 3(d), scattering effect is somewhat suppressed, but the recovery image is not clear due to the fact that the background information is treated as a constant and the noise is amplified during processing. In contrast, our method substantially removed the high-frequency noise of backscattered light by the full spatial low-pass filtering. Even if the milk concentration increases further, clear recovery results are also obtained by our method, which means effectiveness and adaptability to different complex environments of our method. Especially, our method allows for automatic processing of polarized images without human-machine interaction, which are clearly different from manual estimation in Schechner's method.

The grayscale histogram is a function of the distribution of gray levels in an image and it is a count of the frequency of all pixels in a digital image, according to the magnitude of their gray level values. The grayscale histogram reflects the general appearance and quality of the image, and is also an important basis for image enhancement processing, therefore, we plot the results' grayscale distribution histogram of Fig. 3. The corresponding histogram of the results for different concentrations is shown in Fig. 4, where the horizontal and vertical coordinates represent the gray levels and the number of pixels, respectively. It can be seen that the grayscale distribution of the original images affected by high scattering environment is concentrated in

Optics EXPRESS

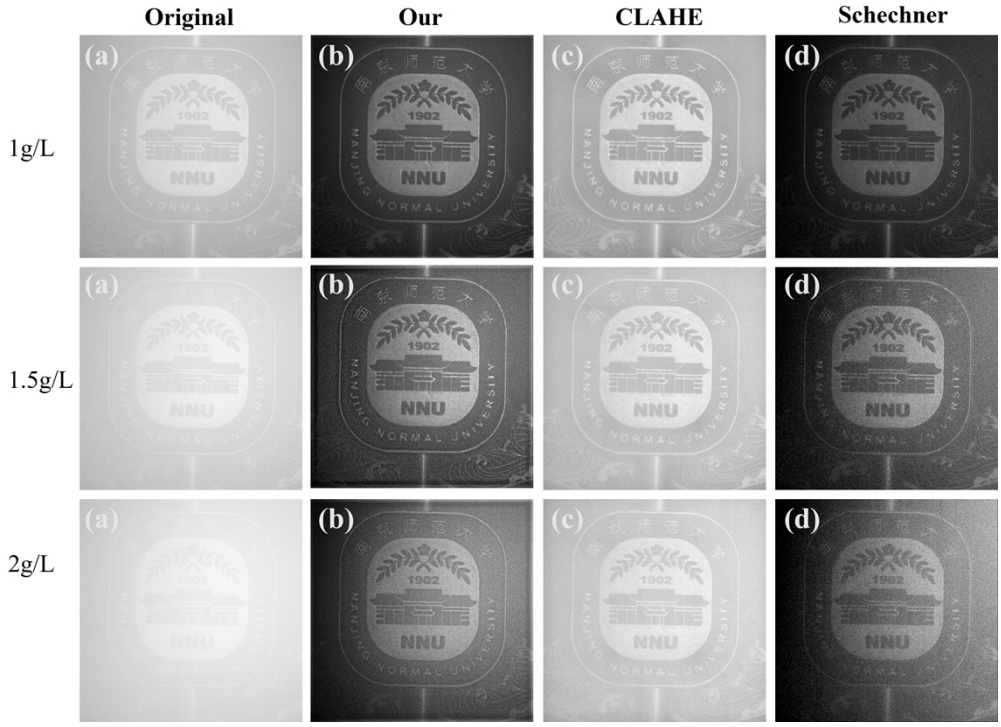

Fig. 3. Recovery results of the different methods under different turbidity conditions. (a) Original turbid image; (b) Results of our method; (c) Results of CLAHE; (d) Results of Schechner's method.

narrow gray areas, which can only be stretched to a finite extent by CLAHE's and Schechner's methods as shown in Fig. 4(c) and (d). However, it is evident that the grayscale distribution of the images recovered by our method shown in Fig. 4(b) is much more uniform and the gray level is much larger than that of the other two methods.

Furthermore, an aluminum ruler and a plastic QR code are chosen as the targets with purpose to test the robustness of different materials of our method, where the milk concentration in the experiments is set at 1.5 g/L. The images of corresponding intensity in clear water, the original turbid images and recovery results are shown in Figs. 5 and 6. From Fig. 6(b), it can be seen that the scale of the ruler and the words 'YS-6415' are clearly distinguishable. It is worth noting that the recovered plastic QR code is not only recognizable to the human eyes, but can also be scanned using a mobile device camera (e.g., mobile phone). Interestingly, Schechner's method gives clearer results for the recovery of aluminum ruler comparing with CLAHE method. However, for plastic QR codes, the CLHAE method has better recovery results and the recovered plastic QR code, which can also be scanned using a mobile device camera. It can be seen that both methods have some dependency on the material of the target, but our method can achieve good recovery results for both materials, which further indicate the superior applicability and robustness of our method.

To objectively quantify the quality of recovery images with different methods, we use full-reference and no-reference image quality evaluation metrics to analyze the recovery results in Fig. 6. The full-reference image quality evaluation index uses the peak signal-to-noise ratio of the image (PSNR) [22], in which the larger PSNR indicates the clearer image. No-reference image

Optics EXPRESS

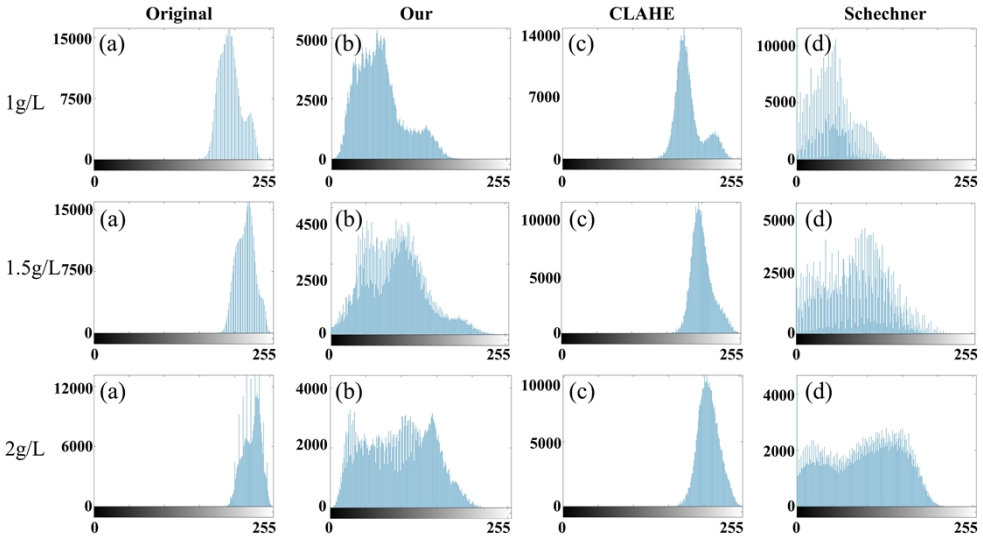

Fig. 4. The histogram of the results for different concentrations and different methods in Fig. 3. (a) Original turbid image; (b) Results of our method; (c) Results of CLAHE; (d) Results of Schechner's method. Where the horizontal coordinate represents the gray levels and the vertical coordinate represents the number of pixels.

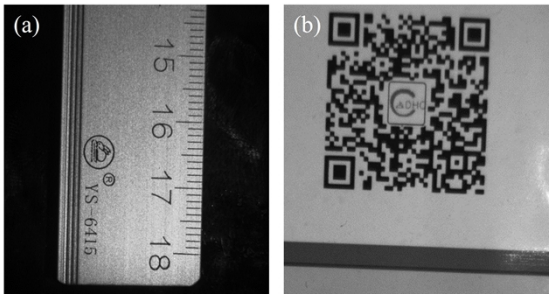

Fig. 5. Image of the target in clear water. (a) Aluminum ruler; (b) QR code.

quality evaluation metrics include contrast ratio [23], the value of the measure of enhancement (EME) and information entropy [24]. The calculation results are shown in Table 1.

Table 1. Quantitative comparison of results in Fig. 6

Different methods	Aluminum ruler				Plastic QR code			
	PSNR	Contrast	EME	entropy	PSNR	Contrast	EME	entropy
Original	4.52	0.09	0.52	5.65	9.51	0.04	0.39	4.83
CLAHE	8.29	0.11	1.83	6.09	10.38	0.07	1.43	5.70
Schechner	8.98	0.28	3.67	6.98	8.86	0.08	1.84	5.92
Our	**13.26**	**0.53**	**6.45**	**7.46**	**15.07**	**0.30**	**5.50**	**7.30**

Among the methods mentioned in Table. 1, the recovery image indexes as PNSR, Contrast, EME and entropy of our method for two targets of different materials are the maximum, where the clarity and detail information of the recovered image are greatly enhanced Interestingly,

Optics EXPRESS

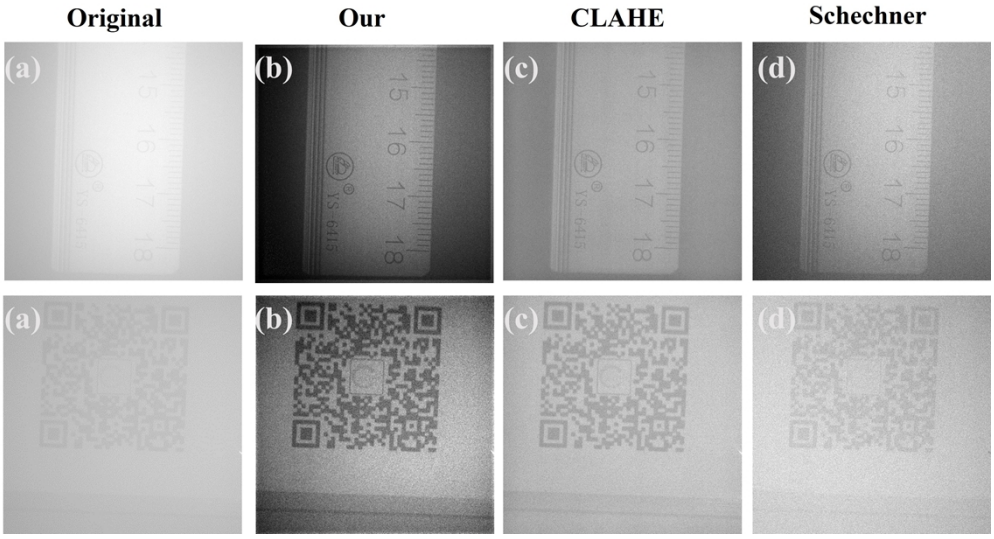

Fig. 6. Targets of different materials in the scattering environment (milk concentration at 1.5 g/L) and recovery by different methods. (a) Original turbid image; (b) Results of our method; (c) Results of CLAHE; (d) Results of Schechner's method.

Schechner's method gives clearer results for the recovery of aluminum ruler comparing with CLAHE method. However, for plastic paper QR codes, the CLHAE method has better recovery results the recovered QR codes, which can also be scanned using a mobile device camera. It can be seen that both methods have some dependency on the material of the target, but our method can achieve good recovery results for both materials, which further indicate the superior applicability and robustness of our method.

Schechner's method requires manually selecting the background to estimate the DOP of backscattered light. This estimation method is very convenient and can obtain clear recovery results under uniformly illuminated environment. But different background regions selected may have a bad impact on the recovery results under non-uniform illumination. What's more, the implementation of manual selection reduces the speed of real-time image processing and make it difficult to use for the recovery of moving targets under turbid water. In this paper, the proposed method can estimate the full spatial distribution of the backscattered light intensity by domain-frequency low-pass filtering, which avoids human-computer interaction and is applicable to environments with non-uniform illumination. Therefore, our method can be applied to the recovery of moving objects because we can process each single image fully automatically. The experimental setup used in Fig. 5(a) is also adopted. We move the ruler horizontally in the tank at a speed of 10 cm/s and capture 50 frames of polarized images continuously by PPC (Maximum frame rate is 75fps) with the frame rate at 40 fps. The average processing time of each frame is around 0.16s with a computer with I5-10400f CPU. The recovery results of some frames (1st, 20th, 30th, 40th and 50th frame) are shown in Fig. 7.

The original image of the ruler moving through the turbid water is shown in Fig. 7(a). Besides the blurring of the target image, we can also see that the light intensity is not uniformly distributed throughout the field of view, with the right side being significantly stronger than the left side. The recovery results of moving target are shown in Fig. 7(b), which indicates that our method not only achieves effective recovery of moving target, but also is not affected by non-uniform illumination.

Optics EXPRESS

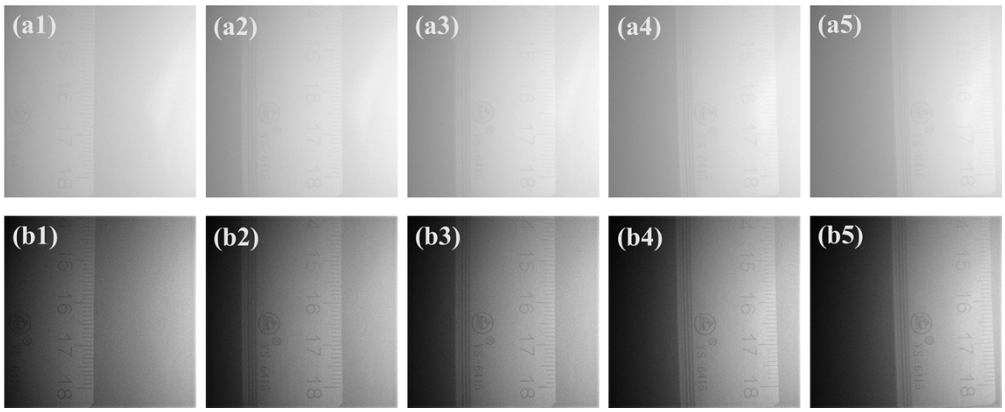

Fig. 7. Five frames of recovery results of moving target. (a) Original turbid image, where the milk concentration is 1.5 g/L; (b) Recovery results. As the target moves through the tank, its image is recovered in real time (see Visualization 1).

4. Conclusion

In this paper, we propose an underwater polarization imaging method for visibility enhancement of moving targets in turbid environments. Firstly, we estimate the full spatial distribution of the backscattered light's intensity and DOP by frequency domain low-pass filter with optimal threshold factor meanwhile the target light's DOP is calculated by using the image evaluation index. At the same time, the histogram stretching technique of polarization relation is used to obtain the polarization images with a larger gray scale. Finally, the calculated DOP of the backscattered light and the target light is substituted into our proposed model to get the recovery images. Experimental studies have been conducted on static and moving targets respectively. The results show that the quality of the recovered results for static targets is significantly improved, with more than 60% improvement in contrast and more than 50% improvement in PSNR compared to traditional method. In additions, moving targets have also been recovered clearly in non-uniform illumination environments. In conclusion, our method estimates the full spatial distribution of backscattered light parameters without human-machine interaction and is adapted to the recovery of moving targets. We believe that this method has great potential in real-time recovery of polarized images in complex underwater environments.

Funding. National Natural Science Foundation of China (11904073, 12174196, 61875093); State Key Laboratory of Applied Optics (SKLAO2022001A17); Natural Science Foundation of Tianjin City (19JCYBJC16500).

Acknowledgments. We are particularly grateful to Prof. Bing Gu (Advanced Photonics Center, Southeast University, Nanjing 210096, China) for refining and polishing the manuscript.

Disclosures. The authors declare no conflicts of interest.

Data availability. Data underlying the results presented in this paper are not publicly available at this time but may be obtained from the authors upon reasonable request.

References

1. G. N. Bailey and N. C. Flemming, "Archaeology of the continental shelf: Marine resources, submerged landscapes and underwater archaeology," Quat. Sci. Rev. **27**(23-24), 2153–2165 (2008).
2. K. Panetta, C. Gao, and S. Agaian, "Human-Visual-System-Inspired Underwater Image Quality Measures," IEEE J. Oceanic Eng. **41**(3), 541–551 (2016).
3. T. T. Ji and G. Y. Wang, "An approach to underwater image enhancement based on image structural decomposition," J. Ocean Univ. China **14**(2), 255–260 (2015).
4. X. Li, Y. L. Han, H. Wang, T. Liu, S. C. Chen, and H. Hu, "Polarimetric Imaging Through Scattering Media: A Review," Front. Phys. **10**, 815296 (2022).

Optics EXPRESS

5. F. Liu, P. Han, Y. Wei, K. Yang, S. Huang, and X. Li, "Deeply seeing through highly turbid water by active polarization imaging," Opt. Lett. **43**(20), 4903–4906 (2018).
6. J. G. Guan, J. P. Zhu, and H. Tian, "Polarimetric Laser Range-Gated Underwater Imaging," Chinese Phys. Lett. **32**(7), 074201 (2015).
7. B. Jwa, B. Mwa, B. Gga, B. Wqa, R. Kan, B. Qha, and C. Qian, "Periodic integration-based polarization differential imaging for underwater image restoration," Opt. Las. Eng. **149**(9), 106785 (2022).
8. H. Wang, J. Li, H. Hu, J. Jiang, and T. Liu, "Underwater Imaging by Suppressing the Backscattered Light Based on Mueller Matrix," IEEE Photonics J. **13**(4), 1–6 (2021).
9. H. Zhang, M. Ren, H. Wang, J. Yao, and Y. Zhang, "Fast processing of underwater polarization imagingbased on optical correlation," Appl. Opt. **60**(15), 4462–4468 (2021).
10. Y. Y. Schechner and N. Karpel, "Recovery of underwater visibility and structure by polarization analysis," IEEE J. Oceanic Eng. **30**(3), 570–587 (2005).
11. Y. Y. Schechner, S. G. Narasimhan, and S. K. Nayar, "Polarization-Based Vision Through Haze," Appl. Opt. **42**(3), 511–525 (2003).
12. B. Huang, T. Liu, H. Hu, J. Han, and M. Yu, "Underwater image recovery considering polarization effects of objects," Opt. Express **24**(9), 9826–9838 (2016).
13. T. Treibitz and Y. Y. Schechner, "Active Polarization Descattering," IEEE Trans. Pattern Anal. Mach. Intell. **31**(3), 385–399 (2009).
14. Y. Zhao, W. He, H. Ren, Y. Li, and Y. Fu, "Polarization descattering imaging through turbid water without prior knowledge," Opt. Las. Eng. **148**, 106777 (2022).
15. H. Hu, L. Zhao, X. Li, H. Wang, and T. Liu, "Underwater image recovery under the non-uniform optical field based on polarimetric imaging," IEEE Photon. J. **10**(1), 1–9 (2018).
16. X. Li, H. Hu, L. Zhao, H. Wang, Y. Yu, L. Wu, and T. Liu, "Polarimetric image recovery method combining histogram stretching for underwater imaging," Sci. Rep. **8**(1), 12430 (2018).
17. F. Feng, G. Wu, Y. Wu, Y. Miao, and B. Liu, "Algorithm for Underwater Polarization Imaging Based on Global Estimation," Acta. Opt. Sin **40**(21), 2111002 (2020).
18. J. Liang, H. Ju, L. Ren, L. Yang, and R. Liang, "Generalized Polarimetric Dehazing Method Based on Low-Pass Filtering in Frequency Domain," Sensors **20**(6), 1729 (2020).
19. D. Robertson and J. J. Dowling, "Design and responses of Butterworth and critically damped digital filters," J Electromyogr Kinesiol **13**(6), 569–573 (2003).
20. H. Wang, H. Hu, J. Jiang, X. Li, W. Zhang, Z. Cheng, and T. Liu, "Automatic underwater polarization imaging without background region or any prior," Opt. Express **29**(20), 31283–31295 (2021).
21. K. Zuiderveld, "Contrast Limited Adaptive Histogram Equalization," Graphics Gems **2**, 474–485 (1994).
22. Q. Huynh-Thu and M. Ghanbari, "Scope of validity of PSNR in image/video quality assessment," Electron. Lett. **44**(13), 800–801 (2008).
23. L. Yang, J. Liang, W. Zhang, H. Ju, L. Ren, and X. Shao, "Underwater polarimetric imaging for visibility enhancement utilizing active unpolarized illumination," Opt. Commun. **438**, 96–101 (2019).
24. R. R. Coifman and M. V. Wickerhauser, "Entropy-based algorithms for best basis selection," IEEE Trans. Inform. Theory **38**(2), 713–718 (1992).